

# Simulations of femtosecond laser pulse interaction with spray target

J. PSIKAL, O. KLIMO, AND J. LIMPOUCH

Czech Technical University in Prague, Faculty of Nuclear Sciences and Physical Engineering, Praha, Czech Republic

(RECEIVED 30 August 2013; ACCEPTED 10 December 2013)

## Abstract

Laser interactions with spray targets (clouds of submicron droplets) are studied here via numerical simulations using two-dimensional particle-in-cell codes. Our simulations demonstrate an efficient absorption of laser pulse energy inside the spray. The energy absorption efficiency depends on the inter-droplet distance, size of the cloud of droplets, and laser pulse intensity, as well as on the pre-evaporation of droplets due to laser pulse pedestal. We investigate in detail proton acceleration from the spray. Energy spectra of protons in various acceleration directions vary significantly depending on the density profile of the plasma created from the droplets and on laser intensity. The spray target can be alternative of foil targets for high intensity high repetition ultrahigh contrast femtosecond lasers. However, at intensities  $>10^{21}$  W/cm<sup>2</sup>, the efficiency of laser absorption and ion acceleration from the droplets drops significantly in contrast to foils.

**Keywords:** Ion acceleration; Laser absorption; PIC simulation; Spray target; Ultrahigh laser intensities

## INTRODUCTION

Interaction of ultrashort high-intensity laser pulses with matter is of great interest in the last two decades due to various observed phenomena, such as acceleration of charged particles (Macchi *et al.*, 2013; Malka, 2012), generation of attosecond pulses (Pukhov, 2003), X-ray or gamma-ray emission (Di Piazza *et al.*, 2012; Nakamura *et al.*, 2012), creation of exotic particles (Ridgers *et al.*, 2012), etc. When intense femtosecond laser pulse irradiates the matter, the ionization threshold is surpassed by many orders of magnitude and plasma is created almost instantaneously. Even at nowadays “moderate” intensities (about  $10^{18}$  W/cm<sup>2</sup>) of the femtosecond laser beam focused into the spot size of several microns, kinetic energy of an electron accelerated in the laser wave electric field can exceed its rest energy. Quasi-static electric fields generated during the interaction of laser pulse with ionized matter can reach values 10000 times larger than the fields applied in conventional particle accelerators. Thus, laser-plasma based accelerators constitute a promising alternative to the conventional ones.

For the studies of femtosecond laser pulse interaction with matter and related particle acceleration, two types of targets are typically used. Gas-jets are usually used for the creation

of underdense plasma, which permits electromagnetic waves to propagate and generate a wakefield accelerating electrons (Malka, 2012). Thin solid foils are usually employed as a source of overdense plasma that transforms the laser pulse energy into accelerated ions efficiently (Macchi *et al.*, 2013). However, alternative targets were also proposed. For example, an efficient source of accelerated ions based on water droplets of diameter of several microns was demonstrated (Nickles *et al.*, 2007). Later, experiments on proton acceleration (Ter-Avetisyan *et al.*, 2008; Ramakrishna *et al.*, 2010) and negative ion generation (Ter-Avetisyan *et al.*, 2011) were carried out with the so-called water spray target that consists of many submicron water micro-droplets (Ter-Avetisyan *et al.*, 2003).

Motivated by the experimental results with the spray target that was proposed as a good candidate for efficient laser energy transfer to the target and thereby for particle acceleration, we investigated the interaction of laser pulse with single submicron droplets (Psikal *et al.*, 2012). We have studied there the dependence of proton acceleration on the laser pulse intensity in the range from  $5 \times 10^{17}$  to  $5 \times 10^{19}$  W/cm<sup>2</sup>, on the laser pulse duration, on the droplet diameter, on initial density profile, and the role of the ionization of submicron water droplet (charge of oxygen ions) was also investigated. A number of other theoretical and numerical studies (Murakami *et al.*, 2006; Ter-Avetisyan *et al.*, 2012; Liseykina & Bauer, 2013) related to the interaction with single

Address correspondence and reprint requests to: Jan Psikal, Faculty of Nuclear Sciences and Physical Engineering CTU, Brehova 7, 115 19 Praha 1, Czech Republic. E-mail: [jan.pszikal@fjfi.cvut.cz](mailto:jan.pszikal@fjfi.cvut.cz)

droplet composed of one or multiple ion species have been published. However, to our knowledge, there are no relevant studies of the interaction between laser and multiple droplets of submicron diameter. In this paper, which is complementary to the previous one (Psikal *et al.*, 2012), we investigate the interaction of femtosecond laser pulse with cloud of such droplets.

Due to computational constraints, we study the interaction in two dimensions, which still gives us insight into the problem. For this study, our two-dimensional particle-in-cell codes with all three velocity components (2D3V) are employed — the first one was developed from one-dimensional LPIC++ code (Pfund *et al.*, 1998) using MPI for parallelization and the second one is our former PIC code (Psikal *et al.*, 2006) used in order to check the results.

## LASER PULSE ABSORPTION AND PROTON ACCELERATION IN THE CLOUD OF SUBMICRON DROPLETS

### Dependence on the Inter-Droplet Distance in Smaller Clouds

In the first set of simulations, we calculated the interaction of femtosecond laser pulse with clouds of uniformly distributed droplets of various mutual distances. The initial droplet diameter was set to 150 nm in agreement with previous experiments (Ter-Avetisyan *et al.*, 2008; Ramakrishna *et al.*, 2010). The water droplet constituents are assumed singly ionized at the start of our simulations (i.e., droplet consists of protons and  $O^{1+}$  ions in ratio 2:1) and the initial electron density is equal to  $19 n_c$  (where  $n_c$  is the critical density) as in Psikal *et al.* (2012). Field ionization of oxygen ions is included in the simulations (for details, see the section about ionization). The laser pulse of amplitude  $a_0 = 3.0$  ( $I = 1.9 \times 10^{19}$  W/cm<sup>2</sup>) has  $\sin^2$  temporal shape of the duration 43 fs ( $16\tau$ , where  $\tau = 2.67$  fs is the laser wave period for the wavelength  $\lambda = 800$  nm). It corresponds to full width at half maximum (FWHM) 20 fs for Gaussian temporal profile. The FWHM of the laser beam is set to  $3.8 \mu\text{m}$  (with Gaussian transverse beam profile). For the maximum initial plasma density, the number of macroparticles in each cell is set to 150 for electrons, 100 for protons, and 50 particles for  $O^{1+}$  ions. All particles have the same weights in the simulations. The cell sizes are equal to 5 nm.

We employed several target configurations for investigations of the influence of the distance between the droplets. The droplets were distributed uniformly with the distance of neighboring droplets (i.e., inter-droplet distance) from  $2 \mu\text{m}$  down to  $0.5 \mu\text{m}$ . The following configurations were used — cloud of  $4 \times 8$  droplets (four rows of eight droplets perpendicularly to the laser pulse propagation direction) for the distance of  $2 \mu\text{m}$  between neighboring droplets (the initial average density of the plasma in the cloud is  $\langle n_e \rangle = 0.096 n_c$ ),  $5 \times 10$  droplets for the distance of  $1.5 \mu\text{m}$  ( $\langle n_e \rangle = 0.17$

$n_c$ ),  $7 \times 15$  for  $1 \mu\text{m}$  ( $\langle n_e \rangle = 0.38 n_c$ ), and  $13 \times 28$  for  $0.5 \mu\text{m}$  ( $\langle n_e \rangle = 1.53 n_c$ ). Note that the average electron density is increased by the factor of about 8/3 (for  $H_2^+O^{6+}$ ) due to the ionization of initial  $H_2^+O^+$  plasma. The number of droplets was varied in order to have similar cloud dimensions in all cases. The size of the cloud is set to be greater than  $13 \mu\text{m}$  in the transverse direction (perpendicular to laser propagation), which is several times larger than the laser beam width in order to take into account the droplets irradiated directly by the incident laser beam and simultaneously the droplets located outside the laser beam in each simulation. We also performed a simulation run with a single droplet of diameter 150 nm for comparison. An example of cloud configuration is shown in Figure 1.

The densities of electrons, protons, and oxygen ions at the end of simulation (about 150 fs after laser-target interaction) are plotted in Figure 2 for inter-droplet distance of  $2 \mu\text{m}$  (cloud of  $4 \times 8$  droplets) in order to illustrate the expansion of droplets after the laser pulse. It can be observed that the droplets irradiated directly by the laser beam expanded rapidly — expanding droplets in the focal spot created underdense plasma (see Fig. 2a). Protons are removed almost completely from the target center in those droplets (see Fig. 2b). Since the proton charge to mass ratio is higher compared to the oxygen ions, the protons are moved by the accelerating electric fields prior to the oxygen ions. Thus, the relative concentration of the oxygen ions in the center of droplets irradiated by a strong laser field is increased (see Fig. 2c). Although the droplets on the sides of the cloud are not irradiated directly by the laser field, they are influenced by escaping hot electrons together with the scattered laser light. In Figure 2b, one can also observe slower expansion of the droplets on the sides. The droplets on the sides expand asymmetrically depending on their position in the cloud — their expansion is faster in the direction outside

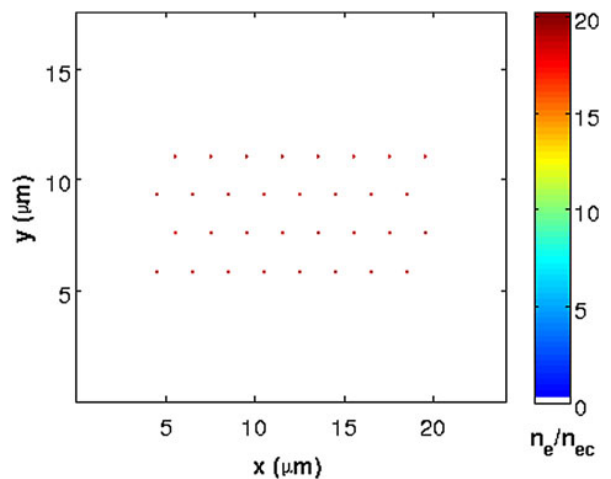


**Fig. 1.** (Color online) Cloud of  $4 \times 8$  droplets of diameter 150 nm in the simulation box. The laser pulse propagates from the bottom to the top. The distance of neighboring droplets (i.e., inter-droplet distance) is  $2 \mu\text{m}$  in this case.

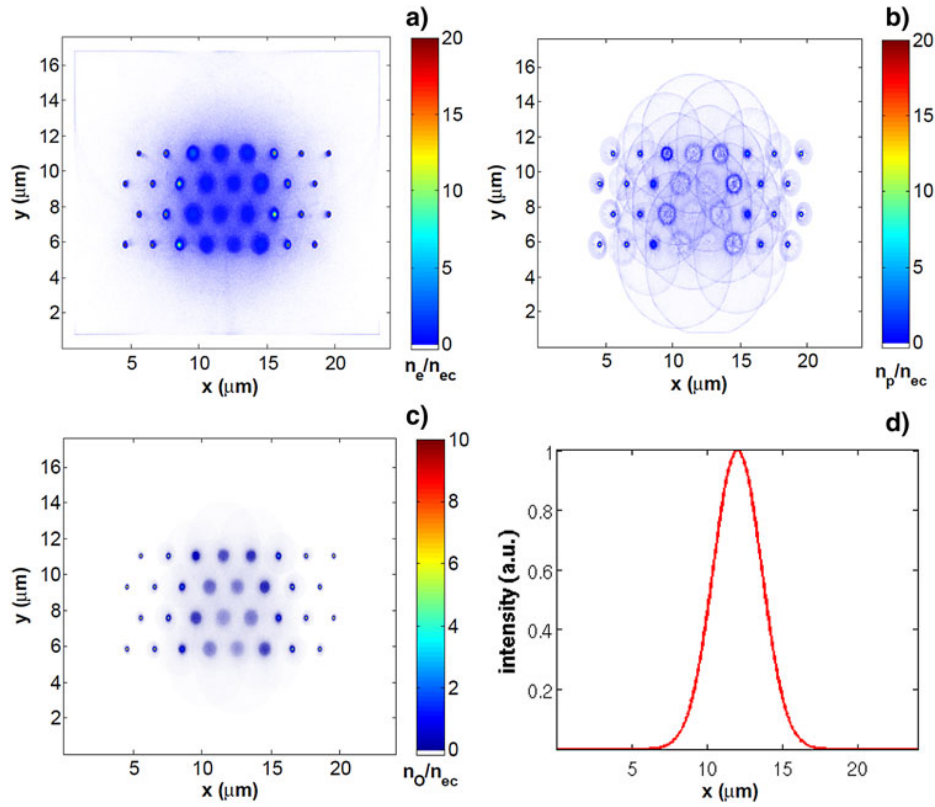


**Fig. 2.** (Color online) (a) Electron, (b) proton, and (c) oxygen ion densities after the irradiation of the cloud of droplets by intense laser pulse of maximum amplitude  $a_0 = 3$  and of the full length of 40 fs. The densities are taken approximately 150 fs after the laser interaction with droplets. (d) Laser beam intensity profile in the direction transverse to the laser pulse propagation.

from the cloud where they are not influenced by other expanding droplets from inner layers of the cloud. Sharp edges in the proton densities of expanded droplets in [Figure 2b](#) indicate a high number of protons accelerated at maximum (cut-off) energies from each submicron droplet.

The energy spectra of protons accelerated in various directions may differ substantially, especially when the interdroplet distance is smaller and a large part of the laser pulse energy is absorbed or reflected on a relatively short distance of several microns. The laser light is strongly absorbed and reflected on the front (laser-irradiated) side of the cloud for denser clouds of sub-wavelength droplets. The laser electric field is presented in [Figure 3](#) at the end of laser-target interaction for inter-droplet distance equal to  $0.5 \mu\text{m}$  (cloud of  $13 \times 28$  droplets). One can see that the reflected laser wave is larger than the wave propagating through the cloud. However, we found that most of the laser pulse energy (about 75%) is absorbed. For the clouds of  $7 \times 15$ ,  $5 \times 10$ , and  $4 \times 8$  droplets, the laser absorption is 57%, 48%, and 34%, respectively, which is a clear indication that the laser wave propagates more easily through the cloud with increasing distance of neighboring droplets. For comparison, the calculated laser absorption is only about 4.5% for a single droplet placed on the axis of the laser beam.

The laser propagation and absorption is strongly related to the ion acceleration. For a single droplet, the maximum energies of protons in various directions differ only slightly. The most favorable direction for the acceleration is about  $60^\circ$  from the laser propagation direction (for the laser pulse

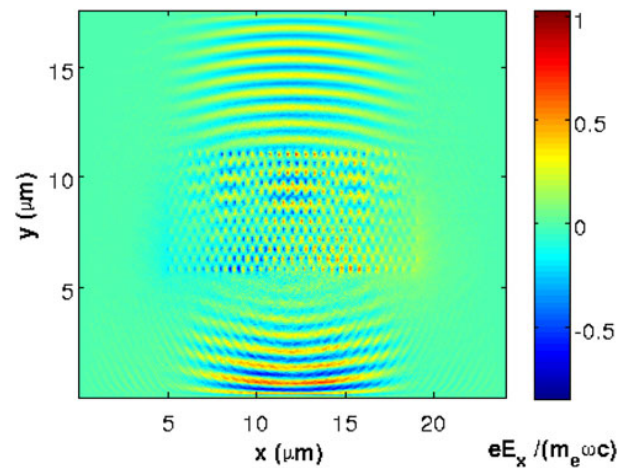


**Fig. 3.** (Color online) Perpendicular (along x-axis) electric field in the simulation box after the interaction of 40 fs laser pulse of amplitude  $a_0 = 3$  with the cloud of  $13 \times 28$  droplets. The inter-droplet distance is  $0.5 \mu\text{m}$ .

amplitude  $a_0 = 3$ ), whereas protons with the lowest maximum energies are accelerated in the opposite direction to the laser propagation (see Fig. 4a). We can ascribe a small difference in various directions to the electron dynamics during laser-droplet interaction — the electrons are ejected from the droplet by oscillating laser field on the cluster sides, but their trajectories are bent toward the laser propagation direction by the laser magnetic field. As a result, the

most energetic protons are observed in an intermediate direction between directions parallel and perpendicular to the laser propagation.

For clouds of droplets, protons with the highest maximum energies are accelerated in the backward direction (opposite ( $180^\circ$ ) — to the laser propagation), although the number of accelerated protons is higher in the forward direction. The relative difference in maximum energies is significant for

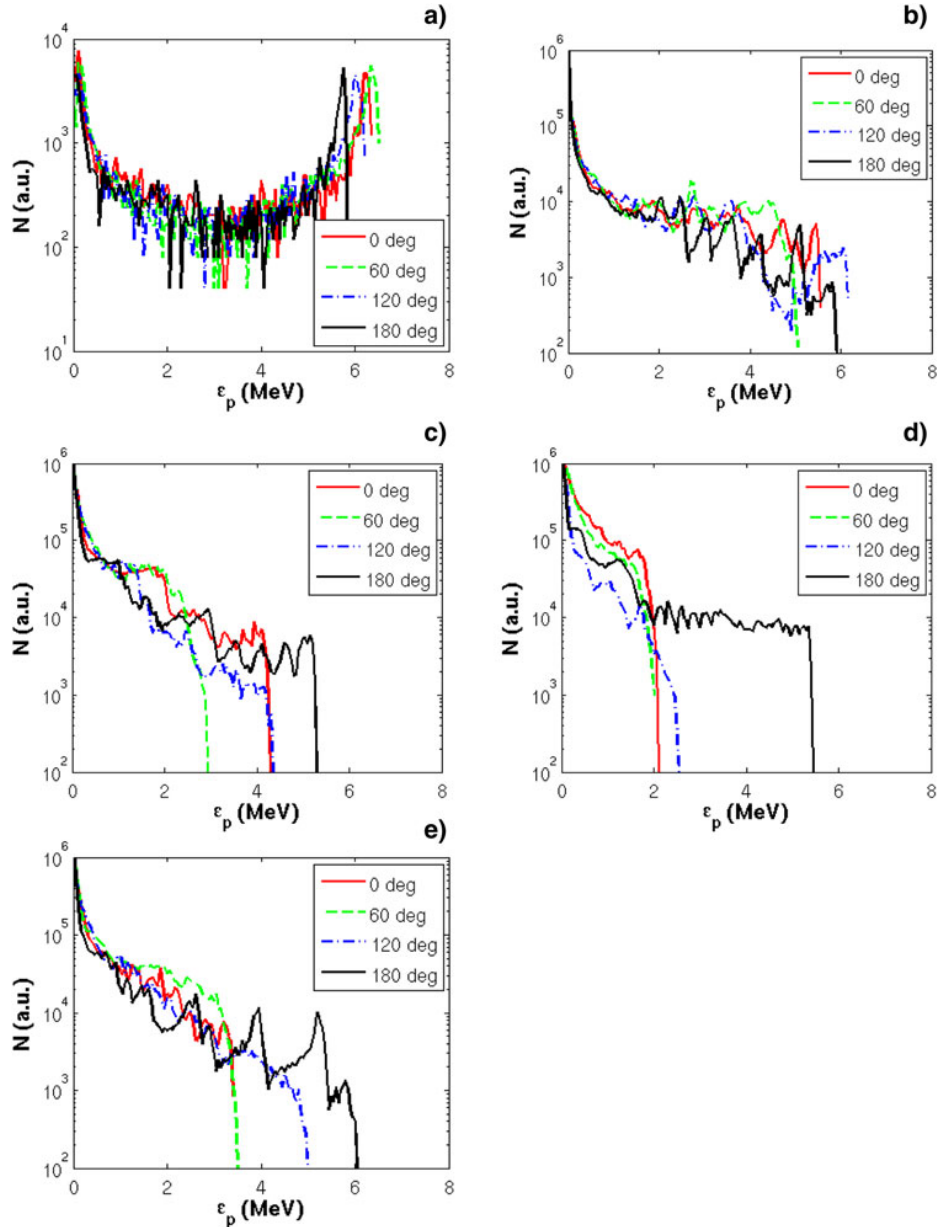


**Fig. 4.** (Color online) Energy spectra of protons accelerated in various directions after the interaction of 40 fs laser pulse of maximum amplitude  $a_0 = 3$  with (a) single droplet of diameter 150 nm, and with the clouds of (b)  $4 \times 8$  droplets, (c)  $7 \times 15$  droplets, (d)  $13 \times 28$  droplets distributed in the simulation box similarly to Figure 1, (e) with the cloud of  $7 \times 15$  droplets in positions on the regular rectangular (Cartesian) grid (inter-droplet distances (b) 2  $\mu\text{m}$ , (c) 1  $\mu\text{m}$ , (d) 0.5  $\mu\text{m}$ , (e) 1  $\mu\text{m}$ ). The angles are measured from the laser propagation direction so “0°” denotes laser pulse propagation (forward) direction and  $180^\circ$  is the backward direction (opposite to laser propagation) and all protons accelerated in the angular range (direction)  $\pm 10^\circ$  around the particular angle are taken into account.

the cloud of  $13 \times 28$  droplets (see Fig. 4d) in contrast to the cloud of  $4 \times 8$  droplets (see Fig. 4b). The difference can be explained by the laser pulse propagation inside the cloud together with electron dynamics in the cloud.

The maximum energy of accelerated protons for single droplet is greater than in cases with multiple droplets since the amount of absorbed energy per particle is the highest in this case. Nevertheless, the maximum energy is one of more parameters describing the efficiency of proton (or, generally, ion) acceleration. Figure 4 shows that the number of accelerated protons is higher for multiple droplets due to a higher total absorption of the laser pulse energy compared with single droplet (but the absorbed energy per particle is lower).

In the case of inter-droplet distance  $2 \mu\text{m}$ , the laser pulse is only slightly absorbed, reflected, or scattered in the front part of the cloud. Then, the droplets on the rear side of the cloud can interact with the laser pulse of similar intensity as on the front side and the protons originating from such droplets are accelerated to roughly same energies. Moreover, the droplets remain clearly separated one from each other for a longer time, even if they expand rapidly. Most of electrons remain bounded to their original droplets (see Fig. 2a). Thus, the acceleration of protons in one droplet is less influenced by other droplets.

For smaller inter-droplet distance  $1 \mu\text{m}$ , the acceleration length of protons is more reduced inside the cloud. In the case of “standard” droplet distribution (see Fig. 1), the maximum energy of ions is larger in the forward direction compared to the case of droplet distribution on the regular Cartesian grid (see Fig. 4c and Fig. 4e). One can explain such difference by the distance of neighboring droplets. For the distribution of droplets presented in Figure 1, the distance of neighboring droplets should be the same (the smallest) in the directions  $30^\circ$ ,  $90^\circ$ , and  $150^\circ$  from the laser propagation direction (in both clockwise or counterclockwise direction since the distribution is symmetrical). For the regular Cartesian droplet distribution, the distance of neighboring droplets is the smallest in the directions  $0^\circ$  (forward) and  $90^\circ$ . One can also observe a slightly higher maximum energy in the backward direction in Figure 4e compared with Figure 4c explained by the position of the first droplet on the central axis of the laser beam and a shift of the droplet position from the axis for the “standard” distribution.

When the distance between droplets is very small ( $0.5 \mu\text{m}$  for the case of  $13 \times 28$  droplets), the maximum energy of forward accelerated protons is substantially smaller compared to the backward direction (see Fig. 4d). In order to understand why the acceleration in the forward direction is limited, one has to take into account two effects. The first one is a strong attenuation of the laser pulse propagating through the cloud of  $13 \times 28$  droplets as it can be seen in Figure 3. Thus, the highest intensity of the laser pulse irradiates the first (front) row of droplets and consequently only protons from this first row can be accelerated to the highest energies. The second effect is the influence of neighboring expanding

droplets on the acceleration (or, in other words, on the expansion of the droplets) as it is demonstrated in Figure 2b, where this effect is apparent mainly for the droplets on lateral sides of the cloud. So, the proton acceleration is limited in the forward direction, but it is not limited in the backward direction (since there are no droplets in front of the first row).

A slightly higher number of protons accelerated in the forward direction compared with the backward direction (even though the proton energies are maximal in the opposite direction) can be explained by a part of hot electrons transported through the cloud. Since the number of accelerated protons depends mainly on the density of hot electrons (Psikal *et al.*, 2010), a higher number of protons is in the forward direction. On the other hand, a higher intensity of laser radiation leads to a higher electron temperature, which is translated rather to the higher maximum proton energy than the number of accelerated protons.

### Dependence on the Size of the Cloud

In this section, we illustrate the efficiency of laser pulse absorption and the attenuation of a focused laser beam inside a thicker cloud of droplets. In order to demonstrate a large absorption of the focused laser beam, larger scale simulations were performed assuming cloud of  $30 \times 8$  droplets distributed uniformly with inter-droplet distance of  $2 \mu\text{m}$  ( $\langle n_e \rangle = 0.096 n_c$ ). The cloud thickness in the laser propagation direction of approximately  $50 \mu\text{m}$  was much greater than about  $5 \mu\text{m}$  for the cloud of  $4 \times 8$  droplets. The laser pulse of the same energy and duration as in the previous case was focused on the cloud rear side with the FWHM focal spot size of  $3.8 \mu\text{m}$  (Gaussian transverse beam profile). Other simulation parameters (droplet size, density, etc.) are the same as in the previous section.

The interaction energy balance is plotted in Figure 5. The laser pulse starts to interact with the cloud at the time  $t_1 = 20\tau$ , where  $\tau$  is the laser period, and the interaction ends at the time  $t_2 \approx 90\tau$ . Already at the interaction half-time ( $t \approx 60\tau$ ), a large part of the laser energy is absorbed. At the end, 90% of the laser pulse energy is absorbed in the plasma created from the droplets. The laser pulse attenuation is illustrated in Figure 6. Focusing of the convergent laser pulse of maximum amplitude  $a_0 \approx 2$  to a narrower beam after propagating of the distance of  $50 \mu\text{m}$  is demonstrated in Figure 6a. However, due to a strong absorption, the final laser pulse amplitude (at simulation time  $t = 80\tau$ ) is only  $a_0 \approx 0.5$  (see Fig 6b). The decrease in laser intensity strongly affects proton acceleration — the maximum energy of protons accelerated in the forward direction is reduced almost two times compared with the thinner cloud of  $4 \times 8$  droplets. This reduction is caused by neighboring expanding droplets that limit the length of proton acceleration area and also by the attenuation of the laser pulse during its propagation through the cloud.

In the case of the thinner cloud composed of  $4 \times 8$  droplets, the laser pulse at the cloud rear edge is intense

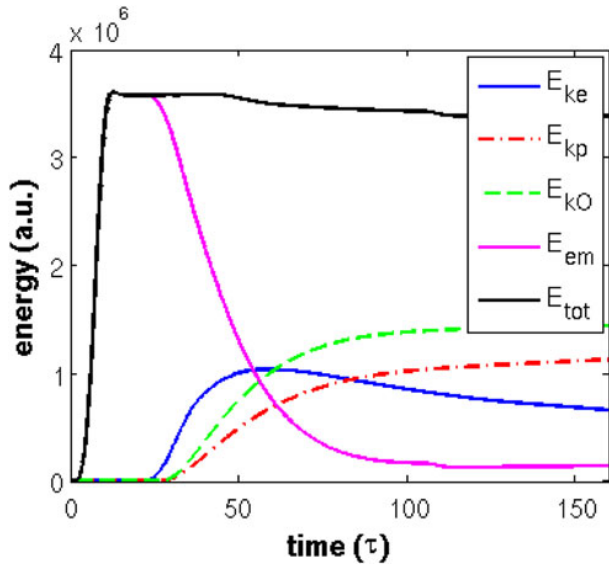


**Fig. 5.** (Color online) Energy balance of the interaction of 40 fs laser pulse of amplitude  $a_0 = 3$  with the cloud of  $30 \times 8$  droplets. The inter-droplet distance is  $2 \mu\text{m}$ . During the laser pulse propagation through the  $50 \mu\text{m}$  thick droplet cloud, 90% of the laser energy is absorbed.  $E_{ke}$  stands for the kinetic energy of electrons,  $E_{kp}$  is the kinetic energy of protons,  $E_{kO}$  denotes the kinetic energy of oxygen ions,  $E_{em}$  is the energy of electromagnetic field inside the simulation box,  $E_{tot}$  is the total energy (of electromagnetic field and particles) inside the simulation box.

enough to accelerate ions to similar energies as at the front edge, whereas the protons are accelerated to much lower energies at the rear edge of the cloud of  $30 \times 8$  droplets. From our simulations, one can estimate that the energies of protons originating from the droplets at rear cloud edge are about an order of magnitude lower than energies of those originating from the front edge. Figure 7a shows energy spectra of protons accelerated in the forward and backward directions. Protons are accelerated to the maximum energy of about 5 MeV in the backward direction compared to about 3 MeV in the forward direction, which can be also explained by the

magnitude of the longitudinal accelerating fields presented in Figure 7b. The laser pulse propagates from the bottom to the top and the pulse position is from  $y \approx 35 \mu\text{m}$  to  $y \approx 48 \mu\text{m}$  at that time moment when the longitudinal fields are imaged. In the region of the pulse, the accelerating fields of relatively high amplitude are generated by electrons expanding from the droplets. Behind the laser pulse, the droplets expanded through each other and the accelerating fields disappeared with the exception of the negative field at the position  $y \approx 15 \mu\text{m}$  at the cloud front edge that accelerates protons further in the backward direction. Such “additional” collective field is responsible for more efficient proton acceleration from the front surface of the cloud compared with the rear surface, but it cannot surpass the highest energy protons in the case of single droplet.

### Comparison of Protons Accelerated From Clouds of Droplets and from Thin-Foils

For laser-induced ion acceleration, thin solid foils are used as the target most frequently. In order to assess the efficiency of proton acceleration from the spray target, we have to compare the energy spectra of protons accelerated from thin-foils and from clouds of droplets. Here, we compare the spectra of protons accelerated in the direction  $0^\circ \pm 10^\circ$  (where  $0^\circ$  is the laser propagation direction for droplets and the target normal direction for thin-foils). For simplicity, the foil target is composed of the same plasma and irradiated by a laser pulse with the same parameters as in the case of clouds of droplets in previous sections. The energy spectra are plotted in Figure 8. While the proton energy distribution function for the cloud of droplets is rather slowly decreasing at higher proton energies up to the maximum (cut-off) energy, the number of protons is exponentially decreasing with increasing energy for thin-foils, in agreement with Mora (2003). Since the proton acceleration in the foils is more efficient at oblique incidence of the laser pulse (Morita et al., 2009), we also present the proton energy

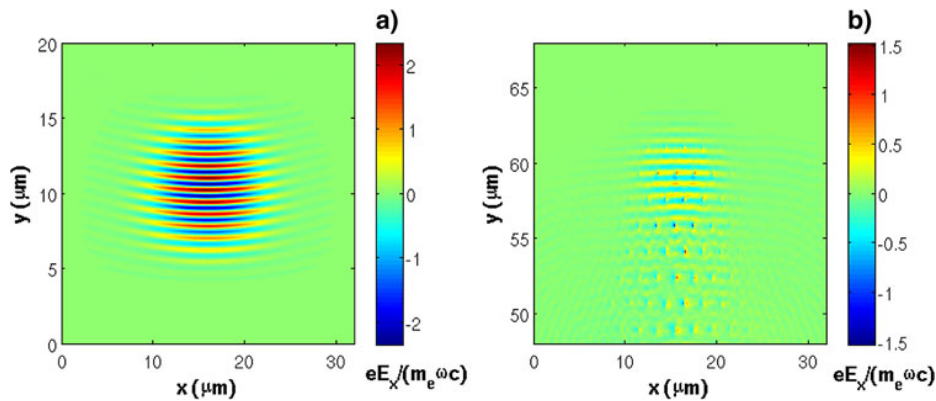


**Fig. 6.** (Color online) Perpendicular (along  $x$ -axis) electric fields of the 40 fs laser pulse (a) before the interaction with the cloud of  $30 \times 8$  droplets, and (b) at the end of the interaction. The cloud extends from  $y = 16 \mu\text{m}$  to  $y = 66 \mu\text{m}$  and the laser focal plane is at  $y = 66 \mu\text{m}$ . However, due to a strong laser absorption in the cloud, the maximum laser amplitude in the projected focal spot is about  $a_0 \approx 0.5$  only.

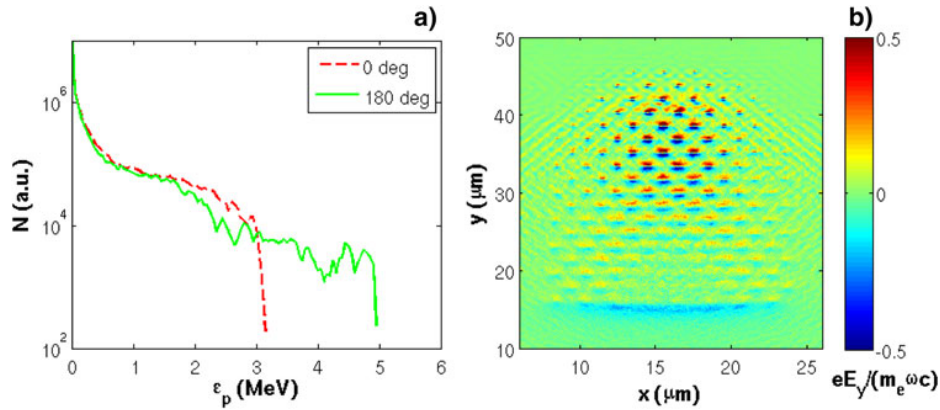


**Fig. 7.** (Color online) (a) Proton energy spectra in the forward ( $0^\circ$ ) and backward ( $180^\circ$ ) directions at the end of simulation of the interaction of 40 fs laser pulse with  $30 \times 8$  droplets (with inter-droplet distance of  $2 \mu\text{m}$ ); (b) Longitudinal electric field (along  $y$ -axis) during the laser pulse interaction with the cloud of  $30 \times 8$  droplets demonstrating the field accelerating protons at the cloud front edge ( $y \approx 15 \mu\text{m}$ ) and in the expanding droplets from  $y \approx 30 \mu\text{m}$  to  $y \approx 45 \mu\text{m}$  (inside the instant laser pulse position).

distribution function from the foil irradiated at the incidence angle of  $30^\circ$ .

One can observe that the protons originated from the cloud of droplets with inter-droplet distance  $2 \mu\text{m}$  (equal to the average distance of droplets in the spray used in previous experiments (Ter-Avetisyan *et al.*, 2008; Ramakrishna *et al.*, 2010)) can be accelerated to higher energies, but their number is substantially lower in the selected direction. Nevertheless, when we compare the absorption of the laser pulse in foils and in droplets, the absorption is more efficient in droplets — for the flat-foil, the absorption is only 4% at normal incidence and 11% at oblique incidence ( $30^\circ$ ),

whereas it is 34% for the cloud of  $4 \times 8$  droplets and 90% for  $30 \times 8$  droplets. Moreover, the number of protons accelerated in the selected solid angle to energies near to the cut-off can be even higher for the thicker cloud ( $30 \times 8$  droplets). The advantage of clouds of droplets is their large surface to volume ratio leading to a higher absorption and their inhomogeneity in space leading to relatively high number of protons accelerated near to the cut-off energy. The main drawback of cylindrical targets in comparison to foil targets is almost isotropic acceleration of protons (Kemp & Ruhl, 2005; Psikal *et al.*, 2008).

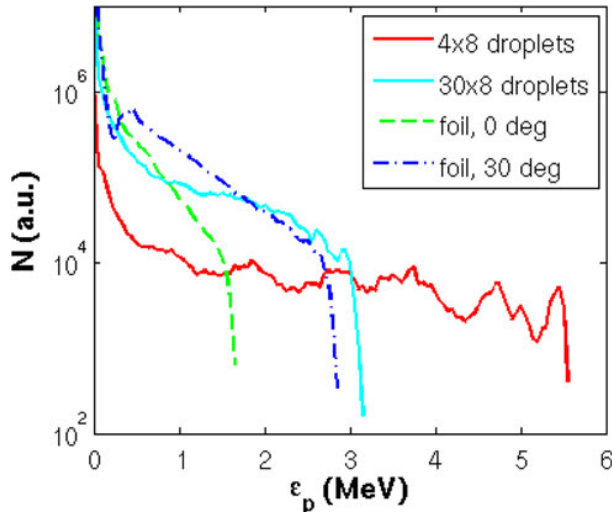


**Fig. 8.** (Color online) Proton energy spectra from the clouds of  $4 \times 8$  droplets and  $30 \times 8$  droplets of diameter  $150 \text{ nm}$  (with inter-droplet distance equal to  $2 \mu\text{m}$ ) and from thin foils of thickness  $150 \text{ nm}$ . The laser beam of amplitude  $a_0 = 3$  and of duration of 40 fs is incident normally ( $0^\circ$ ) on the foil in the first case and at the angle of  $30^\circ$  in the second case. Only protons with divergence less than  $10^\circ$  from the laser forward direction (for droplets) or from the target normal direction (for foils) are taken into account.

### Proton Energy Spectra from Clouds of Pre-Expanded Droplets

We should note that the assumption of sharp droplet boundaries before the arrival of intense femtosecond pulse is valid only for very high laser pulse contrast, probably reaching the value of about  $10^{10}$  achievable by using, e.g., double-plasma mirror (Levy *et al.*, 2007). The proton energy spectra in the experiments (Ter-Avetisyan *et al.*, 2008; Ramakrishna *et al.*, 2010) differ from the spectra displayed in Figure 4. In some shots, a peak close to the maximum proton energy was observed, instead of rather flat or slowly decreasing proton energy distribution function in Figure 4. The laser pulse contrast was reported to be about  $10^8$  in those experiments, which should still lead to some pre-evaporation of the droplets before the arrival of the main laser pulse (Ter-Avetisyan *et al.*, 2012).

If the laser pulse contrast would be very low, the evaporation of droplets would be very large. Then, the created plasma should be almost homogeneous with very low density (less than  $0.05 n_c$  taking into account the average density of water droplets about  $10^{11} \text{ cm}^{-3}$ ). In such case, the laser pulse absorption in plasma would be very low. For example, we calculated absorption slightly above 1% for 40 fs laser pulse of amplitude  $a_0 = 3$  propagating through plasma slab

of electron density  $0.04 n_c$  and thickness  $7.5 \mu\text{m}$ . Consequently, the energies of protons accelerated from such slab with step-like density profile are only about 50 keV. When the laser pulse contrast is increased (from  $10^6$  to  $10^8$  in the experiment), the plasma is inhomogeneous, but it could fill the space with high density variations resulting from partly expanded droplets. Such inhomogeneous plasma cannot be studied in two-dimensional simulations adequately due to a different geometry, and, moreover, the plasma slab of about 1 mm thickness formed in the experiments is too large for PIC simulations. Thus, we can only illustrate an increased absorption and proton acceleration in reduced dimensions of such plasma slab.

In order to mimic the cloud of pre-expanded droplets, we used the configuration of droplets similar to Figure 1, but with overlapping droplets of much larger diameter of about  $3 \mu\text{m}$  with exponential density profile  $n_{\text{max}} \times \exp(-r/L)$ , where the scale length  $L = 1.0\lambda$  and  $n_{\text{max}} = 0.45n_c$ . The total spray mass is the same as for droplets with step-like density profile. The simulation results show the total laser absorption of about 73%, but the energy is translated to ions on a larger time scale than for the droplets with the step-like density profile. At the end of simulation (about 450 fs after laser-target interaction), 30% of the laser energy is translated into protons and oxygen ions.

The energy spectra of protons accelerated in the angular direction  $0^\circ \pm 45^\circ$  from such plasma composed of pre-expanded droplets are displayed in Figure 9. Proton energy spectrum from the cloud of  $4 \times 8$  droplets of step-like density profile is also shown for comparison. Both clouds contain the same number of particles. The energy distribution function originated from the plasma created by pre-expanded droplets includes a peak similar to the experimental results.

In experiments, one can expect that continuous (although inhomogeneous) plasma created from overlapping pre-evaporated droplets is limited transversally by the laser beam width. Thus, the spray consisting of pre-expanded droplets is to some extent similar to an inhomogeneous ‘‘foil section.’’ The modulations (peaks) in proton energy distribution were also observed for foil section targets in previous numerical simulations (see Brantov *et al.*, 2006; Psikal *et al.*, 2008). The peaks were explained by mutual interaction and spatial separation of two ion species. Such modulations were not observed in experiments with foils (Macchi *et al.*, 2013), since the foils were not (sufficiently) limited in the transverse directions and the accelerating field in the sheath was strongly non-uniform (decreasing from the area across the laser spot). On the other hand, quasi-mono-energetic peaks were observed in the experiment with water droplets of diameter  $20 \mu\text{m}$  comparable with laser beam width (Ter-Avetisyan *et al.*, 2006).

### IONIZATION OF SUBMICRON WATER DROPLETS BY PROPAGATING LASER BEAM

In all simulations described above, the field ionization is included using simplified version of the ADK tunneling

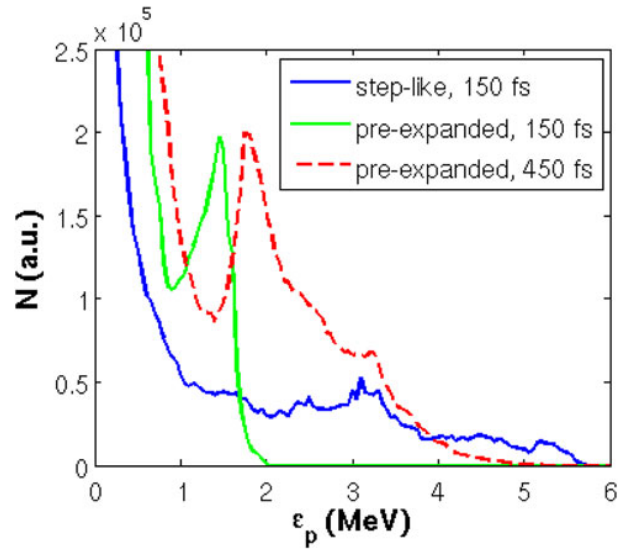


**Fig. 9.** (Color online) Comparison of proton energy spectra in the forward direction from two clouds of  $4 \times 8$  droplets (distance between droplets’ centres is equal to  $2 \mu\text{m}$ ). The first cloud consists of droplets of step-like density profile with initial diameter 150 nm and with the density of water ( $n_{\text{max}} \approx 57n_c$ ). The second cloud consists of strongly pre-expanded (overlapping) droplets of exponential density profile  $n_{\text{max}} \times \exp(-r/L)$ , where  $r$  is the distance from the centre of the droplet,  $L$  is the density scale length, and  $n_{\text{max}}$  stands for maximum initial plasma density ( $L = 0.8 \mu\text{m}$ ,  $n_{\text{max}} = 0.45n_c$ ). The total particle number is the same in both cases. The spectra are taken approximately 150 fs (and 450 fs) after the laser interaction with the droplet cloud. A high peak in the proton energy distribution function at the energy of about 2 MeV is observed in the case of the pre-expanded droplets. The peak is formed from protons accelerated ahead of the heavier ion front.

ionization rate implemented in the code as it was described earlier (Psikal *et al.*, 2012). In this model, the ionization rate  $\omega_A$  is calculated directly from ionization potential  $U_i$ , ion charge  $Z$ , and from the local electric field  $E$ . We also implemented collisional ionization in a similar way as in Klimo (2010). For the calculation of cross-section of collisional ionization, Lotz (1967) formula is employed

$$\sigma_{il} = 4.5 \times 10^{-14} \xi_i \ln\left(\frac{\epsilon_{ke}}{U_i}\right) / (\epsilon_{ke} U_i)$$

where  $\epsilon_{ke}$  is the kinetic energy of electron and  $\xi_i$  is the number of electrons in the outer subshell of ion. The ionization rate is calculated from electron velocities in each cell for all possible ionization states of particles,  $\omega_L = \sum_{\text{electrons}} n_e \sigma_{il} v_e$ , where  $n_e$  is the density of electrons with velocity  $v_e$ . Assuming time step  $dt \ll 1$ , the probability of an ionization event can be expressed as  $\Gamma = (\omega_A + \omega_L) \times dt$ . Since the thresholds for water molecule dissociation, hydrogen, and oxygen atom ionization are relatively low, we started our simulations from  $\text{H}_2^+\text{O}^+$  plasma and we follow the evolution of ionization states of oxygen ions only. If the ionization event takes place, the charge of oxygen ion is increased and new electron is injected into the simulation box on the same place as its parent ion.

In [Figure 10](#), one can observe spatial distribution of average ionization degree of oxygen ions for clouds of (a)  $4 \times 8$ , (b)  $7 \times 15$ , and (c)  $13 \times 28$  droplets (inter-droplet distance of  $2 \mu\text{m}$ ,  $1 \mu\text{m}$ , and  $0.5 \mu\text{m}$ , respectively) in the simulations including only field ionization, and (d) for  $7 \times 15$  droplets in the simulation including both field and collisional ionization. All spatial distributions are taken at the same time moment when the laser pulse ceased to interact with the clouds.

The simulations demonstrate behavior similar to that observed for single droplets in our previous paper (Psikal *et al.*, 2012). For the laser pulse amplitude  $a_0 = 3.0$  and a short pulse duration, there are three layers in the expanding droplet in the laser focal area — outer layer, directly irradiated by the laser field, containing fully stripped  $\text{O}^{8+}$  ions, a thin middle layer containing  $\text{O}^{7+}$  ions, and inner core with  $\text{O}^{6+}$  ions. However, for the neighboring droplet distance of  $0.5 \mu\text{m}$  (less than laser wavelength), only the droplets in the front part of the cloud contain  $\text{O}^{8+}$  ions ([Fig. 10c](#)). In this case, the laser pulse is strongly scattered and attenuated on the front side of the cloud and the laser field is too weak inside the cloud to ionize oxygen atoms to a charge higher than He-like  $\text{O}^{6+}$ . That is due to the fact that the removal of electron from K-shell is more difficult as the ionization potentials of He-like and H-like ion are 739 and 871 eV, respectively, much higher than ionization potential of 140 eV for Li-like oxygen ions.

Ionization degree of oxygen ions is lower outside the area where the laser beam propagates. Here, the ionization takes place due to the electric field generated by the electrons escaping from the laser interaction area and by the scattered laser radiation. In this case, the collisional ionization is also important. We can estimate that, for example, the number of collisional ionization events per one  $\text{O}^{6+}$  ion during the pulse duration (40 fs) is less than  $10^{-2}$  for the temperature of 1 keV and critical density, whereas it is about 0.2 ionization events for  $\text{O}^{4+}$  ion. One can compare [Figures 10b](#) and [10d](#) — collisional ionization affects mainly droplets outside laser beam propagation area on the cloud sides where the average charge of oxygen ions is increased from about 4 to about 6, whereas the charge is only slightly increased in the cloud center. Note that collisional ionization is time consuming in simulations — computational time is increased about more than 50 per cent when it is taken into account. Moreover, the ionization (field and collisional) can be usually omitted in simulations when the proper charge of oxygen ions is assumed (Psikal *et al.*, 2011).

#### LASER INTERACTIONS WITH CLOUD OF SUBMICRON DROPLETS AT ULTRARELATIVISTIC INTENSITIES

Up to now, the interaction of femtosecond laser pulse with the cloud of droplets was investigated only at peak laser

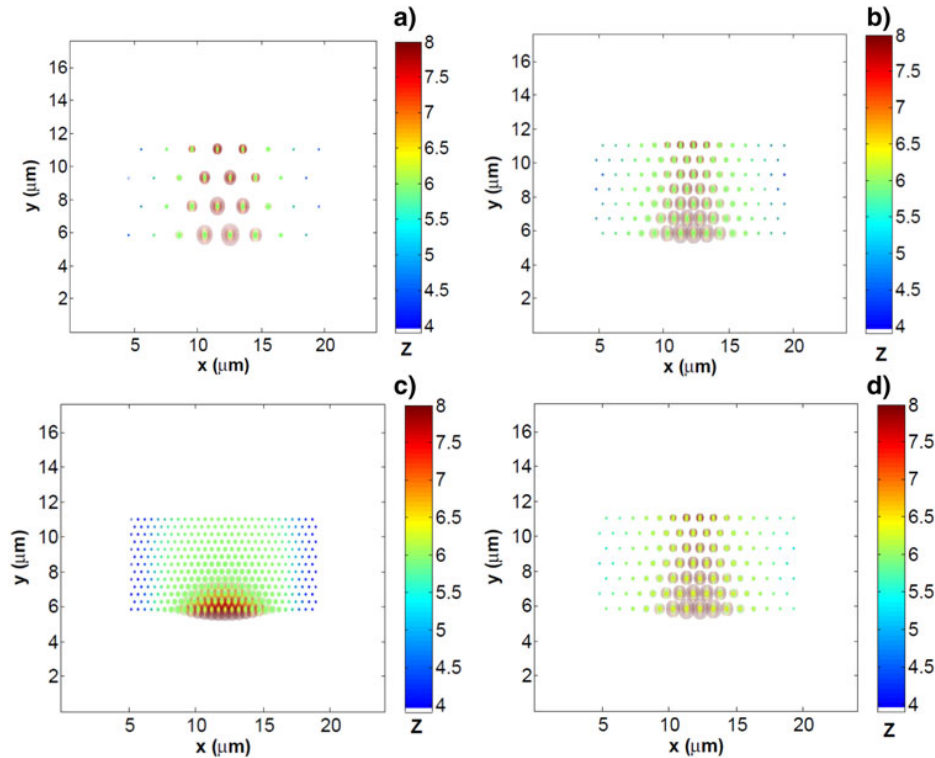


**Fig. 10.** (Color online) Spatial distribution of average ionization degree of oxygen ions after 40 fs laser pulse interaction with clouds of droplets in the case of (a)  $4 \times 8$  droplets, (b)  $7 \times 15$  droplets, (c)  $13 \times 28$  droplets when only field ionization is considered, (d)  $7 \times 15$  droplets when both field and collisional ionization are taken into account.

pulse amplitude  $a_0 = 3$  (intensity  $2 \times 10^{19}$  W/cm<sup>2</sup>). However, laser facilities in the near future will be able to generate femtosecond laser pulses with maximum intensity higher than  $10^{22}$  W/cm<sup>2</sup> (Mourou & Tajima, 2011). Thus, it is desirable to study the interaction at higher intensities. In the following simulations, we used laser pulse amplitudes  $a_0 = 10, 30, 100$  (which means laser intensities  $\approx 2 \times 10^{20}, 2 \times 10^{21}, 2 \times 10^{22}$  W/cm<sup>2</sup>, respectively). All other laser and target parameters remain the same except for the second set of simulations calculated with higher target density.

Due to the relativistically induced transparency and related phenomena (Gibbon & Forster, 1996), the density of plasma could play an important role in the interaction, although the plasma is normally highly overdense. The previous simulations were carried out with the initial target density three times lower than the normal water density. Thus, the electron density was  $19 n_c$  ( $\text{H}_2^+\text{O}^+$  plasma) at the start of our simulations, while the electron density is increased fast to approximately  $50 n_c$  as the majority of oxygen ions is ionized to He-like state. However, the artificial decreased density of water has negligible impact (mainly in terms of absorption and proton energy spectrum) on the interaction for the intensity assumed in previous sections. The comparison is demonstrated in Figure 11 for the case of the cloud of  $4 \times 8$  droplets.

At higher intensities, the electron density is crucial parameter of the interaction. It is well illustrated on laser absorption in various targets shown in Figure 11a. For the droplets of the lower initial density, the absorption rapidly decreases at  $a_0 = 30$ , whereas it drops significantly at  $a_0 = 100$  for the higher density. The absorption in the droplets can be attributed to the evolution of electron densities in the expanding droplets during their interaction with the laser pulse, which was already investigated in our previous work (Psikal *et al.*, 2012). At higher intensities, more electrons are extracted from the droplets during their interaction with the laser pulse and, moreover, the droplets expand rapidly driven by heated electrons. Thus, the density inside droplets is significantly reduced in a time interval shorter than the

laser pulse duration. The plasma becomes transparent before the end of the interaction and the absorption rate is significantly reduced depending on the moment of the plasma transparency. If a large part of electrons is removed, the ions in droplets are subject of Coulomb explosion, which is less efficient than their acceleration driven by hot electrons (Breizman *et al.*, 2005).

We tested the same dependence for thin-foils. Again, the laser and plasma parameters are the same as for droplets, only the target shape is different. For thin-foils and lower initial density, the absorption is relatively high at  $a_0 = 30$  (18% for foil vs. 7% for droplets). Contrary to the droplets, only a small part of electrons can be fully extracted from the foil, and, moreover, the plasma expansion is limited only on the forward direction during the interaction (the expansion in the backward direction starts later, because it is suppressed by the radiation pressure). The plasma density remains higher for a longer time which can explain higher absorption of the laser pulse energy. For the highest amplitude  $a_0 = 100$  and lower plasma density, the foil target is relativistically transparent for the laser wave which can subsequently propagate through the target without significant absorption. For the higher initial plasma density, the foil is not transparent for the laser pulse of amplitude  $a_0 = 100$  and it absorbs 31% of the laser energy (droplets absorb only 2% or 5% of laser energy at such amplitude, depending on their density). When the foil is not transparent for the laser wave, the absorption is increasing with the pulse amplitude. It can be explained by the deformation of the front foil surface during the interaction and efficient  $\mathbf{j} \times \mathbf{B}$  heating. The deformation increases with laser intensity and leads to higher laser pulse absorption.

Maximum proton energy (Fig. 11b) is roughly proportional to the absorbed laser energy. Protons are accelerated to maximum energies of 6 MeV, 18 MeV, 30 MeV, 42 MeV in the droplets of lower initial densities irradiated by laser pulses of amplitudes  $a_0 = 3, 10, 30, 100$ , respectively. Protons of energies 6 MeV, 65 MeV, and 130 MeV

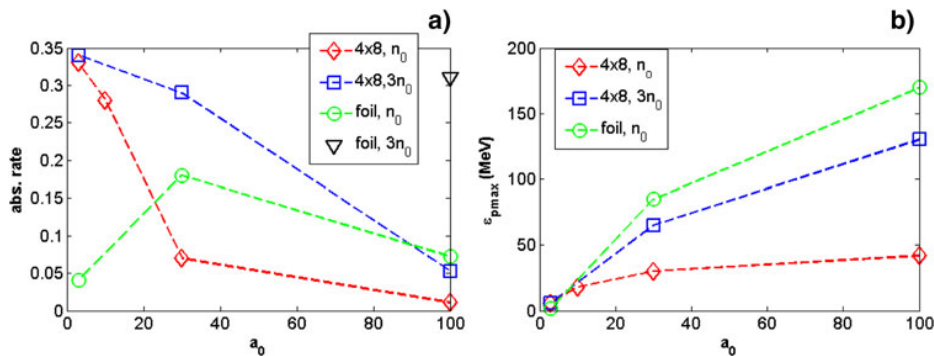


**Fig. 11.** (Color online) (a) The dependence of laser absorption in various targets (cloud of  $4 \times 8$  droplets and the foil irradiated at normal incidence with lower —  $n_0$  — and higher —  $3n_0$  — target densities) on the laser pulse amplitude  $a_0$ ; (b) The dependence of the maximum proton energy  $\epsilon_{pmax}$  on the laser amplitude  $a_0$ . The higher target density corresponds to the real water density. The droplets are of step-like density profiles with diameter 150 nm, the foil thickness is equal to 150 nm.

protons are observed for the droplets of higher initial densities and  $a_0 = 3, 30, 100$ . One can see that even if the laser intensity (proportional to  $a_0^2$ ) is increased by about one order of magnitude, proton energies are increased by factor 1.4 or 2 at the highest intensities assumed here. The proton energies from the foil of lower initial density are 2 MeV, 85 MeV, 170 MeV for  $a_0 = 3, 30, 100$ , respectively, whereas the protons are accelerated up to 520 MeV for the highest amplitude and the higher initial target density which is caused by relatively high absorption of the laser energy in this case.

With increasing laser intensity, proton acceleration and droplet expansion starts to be strongly asymmetric. Energy spectra of protons accelerated from denser droplets at laser amplitude  $a_0 = 100$  are shown in Figure 12. The protons reach energy up to 130 MeV in the forward direction, whereas it is only about 65 MeV in the backward direction. Also the number of accelerated protons to energies higher than 1 MeV is almost three times higher in the forward than in the backward direction. This anisotropy can be explained by electron dynamics. With increasing laser intensity, more electrons are extracted earlier from the droplets and accelerated in the direction of the laser pulse propagation.

## CONCLUSIONS

We have demonstrated by two-dimensional PIC simulations that laser pulse energy can be efficiently absorbed in the cloud of submicron droplets (the so-called spray target) — for example, 90% of the energy of 40 fs laser pulse of intensity about  $10^{19}$  W/cm<sup>2</sup> is absorbed in 50  $\mu$ m thick cloud of droplets with inter-droplet distance equal to 2  $\mu$ m in the

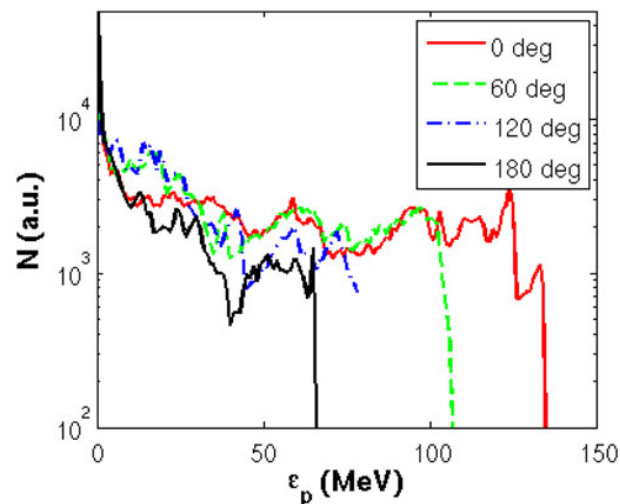


**Fig. 12.** (Color online) Proton energy spectra in various directions with respect to the laser propagation direction ( $0^\circ$ ) after the interaction of 40 fs laser pulse of amplitude  $a_0 = 100$  with the cloud of  $4 \times 8$  droplets. The initial density of droplets with diameter 150 nm is equal to the real water density.

simulation plane. Such strong laser absorption and strong inhomogeneity of the target lead to relatively efficient ion acceleration, although the ions are accelerated in all directions with a relatively low anisotropy. The anisotropy of the acceleration is increased with decreasing inter-droplet distance, with increasing cloud thickness, and with growing laser pulse intensity.

In experiment, the droplets can be strongly pre-evaporated due to the laser pulse pedestal (insufficient laser pulse contrast) which has significant influence on the proton energy spectra. Plasma composed of pre-evaporated droplets before the arrival of the main laser pulse can behave similarly to the foil section (limited in transverse dimensions owing to laser propagation direction) and the peak in proton energy spectra near the cut-off energy can be formed due to the interaction between multiple ion species and their different charge-to-mass ratio.

When ultrahigh laser pulse contrast is assumed and femtosecond laser pulse interacts with targets of step-like density profile, the energies and numbers of high-energy protons accelerated from foils and from clouds of droplets can be comparable in the direction normal to the foil surface. The advantage of the spray target is a relatively high number of ions accelerated near maximum (cut-off) energy and also ease of its use for high-repetition rate femtosecond lasers. However, laser absorption and the efficiency of proton acceleration are reduced at ultrahigh laser intensities ( $I > 10^{21}$  W/cm<sup>2</sup>). At such high laser amplitudes, electrons are almost completely removed from submicron droplets and the acceleration is driven mainly by Coulomb explosion contrary to the thin-foils up to the moment when the foil becomes relativistically transparent.

## ACKNOWLEDGEMENTS

This research has been supported by the Czech Science Foundation project P205/12/P366 and partially by the Ministry of Education, Youth, and Sports of the Czech Republic project LG13029. Parallel computing resources have been partially provided by Helmholtz-Zentrum Dresden-Rossendorf (HZDR), Germany. The authors would like to express their gratitude to Dr. Michael Bussmann and to his colleagues from HZDR for fruitful discussions about parallel computing.

## REFERENCES

- BRANTOV, A.V., TIKHONCHUK, V.T., KLIMO, O., ROMANOV, D.V., TER-AVETISYAN, S., SCHNURER, M., SOKOLLIK, T. & NICKLES, P.V. (2006). Quasi-mono-energetic ion acceleration from a homogeneous composite target by an intense laser pulse. *Phys. Plasmas* **13**, 122705.
- BREIZMAN, B.N., AREFIEV, A.V. & FOMYTSKYI, M.V. (2005). Non-linear physics of laser-irradiated microclusters. *Phys. Plasmas* **12**, 056706.
- DI PIAZZA, A., MULLER, C., HATSAGORTSYAN, K.Z. & KEITEL, C.H. (2012). Extremely high-intensity laser interactions with fundamental quantum systems. *Rev. Mod. Phys.* **84**, 1177–1228.

- GIBBON, P. & FORSTER, E. (1996). Short-pulse laser-plasma interactions. *Plasma Phys. Control. Fus.* **38**, 769–793.
- KEMP, A.J. & RUHL, H. (2005). Multispecies ion acceleration off laser-irradiated water droplets. *Phys. Plasmas* **12**, 033105.
- KLIMO, O. (2010). *PIC Simulations of Ultrashort-Pulse Laser Solid-Target Interactions: The Role of Collisions and Ionization*. Saarbrücken, Germany: Lambert Academic Publishing.
- LEVY, A., CECCOTTI, T., D'OLIVEIRA, REAU, F., PERDRIX, M., QUERE, F., MONOT, P., BOUGEARD, M., LAGADEC, H., MARTIN, P., GEINDRE, J.P. & AUDEBERT, P. (2007). Double plasma mirror for ultrahigh temporal contrast ultraintense laser pulses. *Opt. Lett.* **32**, 310–312.
- LISEYKINA, T.V. & BAUER, D. (2013). Plasma-formation dynamics in intense laser-droplet interaction. *Phys. Rev. Lett.* **110**, 145003.
- LOTZ, W. (1967) An empirical formula for the electron-impact ionization cross-section. *Z. Physik* **206**, 205–211.
- MACCHI, A., BORGHESI, M. & PASSONI, M. (2013). Ion acceleration by superintense laser-plasma interaction. *Rev. Mod. Phys.* **85**, 751–793.
- MALKA, V. (2012). Laser plasma accelerators. *Phys. Plasmas* **19**, 055501.
- MORA, P. (2003). Plasma expansion into a vacuum. *Phys. Rev. Lett.* **90**, 185002.
- MORITA, T., ESIRKEPOV, T.Z., KOGA, J., YAMAGIWA, M. & BULANOV, S.V. (2009). The effect of laser pulse incidence angle on the proton acceleration from a double-layer target. *Plasma Phys. Contr. Fus.* **51**, 024002.
- MOUROU, G. & TAJIMA, T. (2011). More intense, shorter pulses. *Sci.* **331**, 41–42.
- MURAKAMI, M. & BASKO, M.M. (2006). Self-similar expansion of finite-size non-quasi-neutral plasmas into vacuum: Relation to the problem of ion acceleration. *Phys. Plasmas* **13**, 012105.
- NAKAMURA, T., KOGA, J.K., ESIRKEPOV, T.Z., KANDO, M., KORN, G. & BULANOV, S.V. (2012). High-power gamma-ray flash generation in ultraintense laser-plasma interactions. *Phys. Rev. Lett.* **108**, 195001.
- NICKLES, P.V., TER-AVETISYAN, S., SCHNUEERER, M., SOKOLLIK, T., SANDNER, W., SCHREIBER, J., HILSCHER, D., JAHNKE, U., ANDREEV, A. & TIKHONCHUK, V. (2007). Review of ultrafast ion acceleration experiments in laser plasma at Max Born Institute. *Laser Part. Beams* **25**, 347–363.
- PFUND, R.E.W., LICHTERS, R. & MEYER-TER-VEHN, J. (1998). LPIC ++ a parallel one-dimensional relativistic electromagnetic particle-in-cell code for simulating laser-plasma-interaction. *AIP Conf. Proc.* **426**, 141–146.
- PSIKAL, J., LIMPOUCH, J., KAWATA, S. & ANDREEV, A.A. (2006). PIC simulations of femtosecond interactions with mass-limited targets. *Czech. J. Phys.* **56**, B515–B521.
- PSIKAL, J., TIKHONCHUK, V.T., LIMPOUCH, J., ANDREEV, A.A. & BRANTOV, A.V. (2008). Ion acceleration by femtosecond laser pulses in small multispecies targets. *Phys. Plasmas* **15**, 053102.
- PSIKAL, J., TIKHONCHUK, V.T., LIMPOUCH, J. & KLIMO, O. (2010). Lateral hot electron transport and ion acceleration in femtosecond laser pulse interaction with thin foils. *Phys. Plasmas* **17**, 013102.
- PSIKAL, J., KLIMO, O. & LIMPOUCH, J. (2011). Field ionization effects on ion acceleration in laser-irradiated clusters. *Nucl. Instrum. Meth. Phys. Res. A* **653**, 109–112.
- PSIKAL, J., KLIMO, O. & LIMPOUCH, J. (2012). 2D particle-in-cell simulations of ion acceleration in laser irradiated submicron clusters including field ionization. *Phys. Plasmas* **19**, 043107.
- PUKHOV, A. (2003). Strong field interaction of laser radiation. *Rep. Prog. Phys.* **66**, 47–101.
- RAMAKRISHNA, B., MURAKAMI, M., BORGHESI, M., EHRENTAUF, L., NICKLES, P.V., SCHNUEERER, M., STEINKE, S., PSIKAL, J., TIKHONCHUK, V. & TER-AVETISYAN, S. (2010). Laser-driven quasimonoenergetic proton burst from water spray target. *Phys. Plasmas* **17**, 083113.
- RIDDERS, C.P., BRADY, C.S., DUCLOUS, R., KIRK, J.G., BENNETT, K., ARBER, T.D., ROBINSON, A.P.L. & BELL, A.R. (2012). Dense electron-positron plasmas and ultraintense gamma rays from laser-irradiated solids. *Phys. Rev. Lett.* **108**, 165006.
- TER-AVETISYAN, S., SCHNUEERER, M., STIEL, H. & NICKLES, P.V. (2003). A high-density sub-micron liquid spray for laser driven radiation sources. *J. Phys. D: Appl. Phys.* **36**, 2421–2426.
- TER-AVETISYAN, S., SCHNUEERER, M., NICKLES, P.V., SMIRNOV, M.B., SANDNER, W., ANDREEV, A., PLATONOV, K., PSIKAL, J. & TIKHONCHUK, V. (2008). Laser proton acceleration in a water spray target. *Phys. Plasmas* **15**, 083106.
- TER-AVETISYAN, S., RAMAKRISHNA, B., BORGHESI, M., DORIA, D., ZEPF, M., SARRI, G., EHRENTAUF, L., ANDREEV, A., NICKLES, P.V., STEINKE, S., SANDNER, W., SCHNUEERER, M. & TIKHONCHUK, V. (2011). MeV negative ion generation from ultra-intense laser interaction with a water spray. *Appl. Phys. Lett.* **99**, 051501.
- TER-AVETISYAN, S., RAMAKRISHNA, B., PRASAD, R., BORGHESI, M., NICKLES, P.V., STEINKE, S., SCHNUEERER, M., POPOV, K.I., RAMUNNO, L., ZMITRENKO, N.V. & BYCHENKOV, V.Y. (2012). Generation of a quasi-monoenergetic proton beam from laser-irradiated submicron droplets. *Phys. Plasmas* **19**, 073112.